CONFIDENTIAL

NACA

RESEARCH MEMORANDUM

for the

U. S. Army Ordnance

EFFECT OF ROCKET-MOTOR OPERATION ON THE DRAG OF THREE

1/5-SCALE HERMES A-3A MODELS IN FREE FLIGHT

By H. Herbert Jackson

Langley Aeronautical Laboratory
Langley Field, Va.

CLASSIFICATION CHANGED

UNCLASSIFIED

To _____

By authority of _Nasa TPA 8_ Date _7-22-59_ Effective

NB 9-14-59

NATIONAL ADVISORY COMMITTEE
FOR AERONAUTICS
WASHINGTON

CONFIDENTIAL
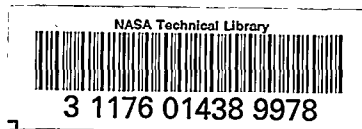
NATIONAL ADVISORY COMMITTEE FOR AERONAUTICS

RESEARCH MEMORANDUM

for the

U. S. Army Ordnance

EFFECT OF ROCKET-MOTOR OPERATION ON THE DRAG OF THREE

1/5-SCALE HERMES A-3A MODELS IN FREE FLIGHT

By H. Herbert Jackson

SUMMARY

Three 1/5-scale models of the Hermes A-3A missile have been flown to determine the effect of rocket-motor operation on the drag corresponding to various altitude and Mach number combinations. The flights covered a Mach number range from 0.5 to 1.8, and ratios of jet-exit static pressure to free-stream static pressure from 0.8 to 1.8.

The results indicate that the power-on drag of the missile should be the same as the power-off drag at Mach number 1.3 and slightly less than the power-off drag at Mach number 1.55.

INTRODUCTION

The Project Hermes is being conducted by the General Electric Company under the direction of the Office of the Chief of Ordnance, Department of the Army. One phase of this program consists of the development of a short-range (80 miles) surface-to-surface missile called the Hermes A-3A. This missile is to be propelled by a large single-stage, liquid-fuel rocket motor.

Available data in references 1 and 2 indicate that jet-on base drag for a given Mach number can vary greatly with the ratio of jet-exit pressure to free-stream pressure and with the geometric configuration of the afterbody.

Inasmuch as the range and performance of the Hermes A-3A are critically dependent on the power-on base pressure and drag, the National Advisory Committee for Aeronautics was requested by the Office of the

Chief of Ordnance, Department of the Army, to measure these quantities
during powered and coasting flights of several 1/5-scale Hermes A-3A
solid-propellant rocket models. These models were to be designed and
flight tested in such a manner as to make the test conditions closely
simulate those of the full-scale Hermes A-3A. This was done by using
the same external model configuration, maintaining a ratio of jet-exit
diameter to model base diameter equal to that of the full-scale model,
and obtaining ratios of jet-exit static pressure to free-stream static
pressure similar to those measured on the full-scale model. The full-
scale missile, because of the high-altitude trajectory flown and the
resulting change in free-stream pressure, has a jet-exit to free-stream
pressure ratio which varies greatly with Mach number. It was necessary,
however, to flight-test the small-scale solid-propellant models at rela-
tively much lower altitudes; therefore, several models were tested, each
with a different value of exit pressure, in order to cover the combina-
tions of jet-exit to free-stream pressure ratios and Mach numbers obtained
for the full-scale missile. These tests were conducted at the Langley
Pilotless Aircraft Research Station at Wallops Island, Va.

The data are presented over a Mach number range from approximately
0.5 to 1.8 and cover a Reynolds number range of 20×10^6 to 60×10^6,
based on body length.

SYMBOLS

C_{D_T} total drag coefficient, based on maximum cross-sectional
area of body

C_{D_B} base drag coefficient, referred to maximum cross-sectional
area of body; for power on, $\dfrac{p_b - p_\infty}{q} \dfrac{A_a}{A_{max}}$; for power off,

$\dfrac{p_b - p_\infty}{q} \dfrac{A_b}{A_{max}}$

C_T thrust coefficient, T/qA_{max}

$\dfrac{\Delta p}{q}$ side-pressure coefficient, $\dfrac{p_s - p_\infty}{q}$

$\dfrac{p_b - p_\infty}{q}$ base-pressure coefficient

M Mach number
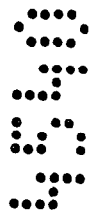
R	Reynolds number, based on body length (5.733 ft)
p_∞	free-stream static pressure, lb/sq ft
p_b	base pressure, measured on base annulus (45° between fins), lb/sq ft
p_s	side pressure, measured on boattail (45° between fins), lb/sq ft
p_e	rocket-motor-exit static pressure, lb/sq ft
A_a	annular area between rocket nozzle and model base (0.0766 sq ft)
A_b	total base area (0.1257 sq ft)
A_{max}	maximum cross-sectional area of body (0.349 sq ft)
A_e	nozzle-exit area (0.0491 sq ft)
A_t	nozzle-throat area, sq ft
T	rocket-motor thrust, lb
q	dynamic pressure, lb/sq ft

MODELS AND TESTS

The general configuration of the 1/5-scale Hermes A-3A test models is given in figure 1. The fins for model C, as can be seen from the figure, were approximately 30 percent larger than those of models A and B. Photographs of one of the test models are shown in figure 2 and a photograph of a model in launching position is shown in figure 3.

The models were constructed of laminated mahogany with a brass nose plug and aluminum-alloy tail section and fins. The wood portions of test models A and B were finished with clear lacquer, whereas model C was finished with Phenoline-300, a commercial preparation which is able to withstand the more severe aerodynamic heating associated with the higher Mach numbers.

In order to simulate full-scale test conditions as closely as possible, 1/5-scale jet vanes were fixed into place at the base of the model as shown in figure 2. These vanes were of steel and were nonmovable.

Figure 4(a) shows a set of jet vanes prior to and after being used in the static test of the sustainer rocket motor for model B. The erosion, melting, and oxidation that took place are shown in figure 4(b). Each vane showed an average loss in effective area of approximately 15 percent and an average loss in weight of about 1.2 percent. This loss in effective vane area is about what would be expected on the full-scale missile.

A two-stage propulsion system was employed for all models presented herein, and all models utilized a modified 5-inch British Cordite rocket motor as the sustainer unit. The modifications to the motor varied with the model and are shown in figure 5. Various booster rocket motors were utilized to obtain the Mach numbers desired. Models A, B, and C used a 3.25-inch MK 7 aircraft rocket motor, a 5-inch HVAR light weight, and a lengthened 5-inch rocket motor, respectively, for boosters. Each booster was equipped with four stabilizing fins and engaged the model by means of a female-type adapter.

Data were obtained for the accelerating portions of flight during sustainer-rocket-motor burning and for the decelerating portions after sustainer-rocket-motor burnout. Trajectory and atmospheric data were obtained from an SCR 584 tracking radar unit and by radiosonde observations. Velocity and total drag were obtained from CW Doppler radar as described in reference 3 and from data telemetered to a ground receiving station by instrumentation incorporated within the models. Thrust coefficient, base drag, and side pressure were obtained from telemetered data.

Base pressure for the models was measured on the model base annulus $45°$ between the fins and jet vanes as is shown in figure 2. The base drag was computed with the assumptions that while the sustainer rocket motor was firing the measured base pressure acted over the annular area of the base, and that after sustainer burnout the measured base pressure acted over the entire area of the base. The side pressure was measured by an orifice located $45°$ between the fins, 1 base diameter (4.8 in.) forward of the base for model A and 1/2 base diameter (2.4 in.) forward of the base for model B. The sustainer-rocket-motor chamber pressure for the models was measured by an orifice located at the beginning of the convergent section of the nozzle. The rocket-motor-exit static pressure was measured by an orifice located ahead of the nozzle exit, 0.064 inch for model A and 0.875 inch for models B and C, and then corrected to the exit.

The thrust of the rocket motor was calibrated as a function of chamber and nozzle-exit pressures in preflight static tests. The thrust in flight was obtained by means of this static calibration and the rocket chamber and nozzle-exit pressures which were measured during flight. The flight thrust and free-stream conditions were then used in determining the thrust coefficient C_T of the model.

The variation of flight dynamic pressure with Mach number for the test models is presented in figure 6.

The Reynolds numbers obtained in flight are plotted against Mach number in figure 7. The flight tests covered a range of body-length Reynolds numbers from 20×10^6 to 60×10^6 and Mach numbers from 0.5 to 1.8.

PROBABLE ERRORS

The main sources of error in the determination of drag coefficient as a function of Mach number are inaccuracies in the instruments and in the reduction of instrument-recorded data. A probable error has been obtained by a consideration of instrument accuracy and of the probable error involved in the data-reduction system.

The probable error in the faired curves of total drag coefficient and base drag coefficient presented herein is less than ± 0.007 and ± 0.005, respectively. The probable error in Mach number is less than ± 0.01.

RESULTS AND DISCUSSION

The variation of thrust coefficient, based on body frontal area, with Mach number for the test models is presented in figure 8. The thrust coefficient shown for model A covered only a Mach number range of 0.8 to 1.0 because of malfunctioning of the flight chamber-pressure pickup over the remaining Mach number range of the model.

Shown in figure 9 is the variation of p_e/p_∞, the ratio of jet-exit pressure to atmospheric pressure, as obtained for the test models in flight. Also shown is a plot of p_e/p_∞ against Mach number corresponding to the full-scale missile trajectory.

The high ratios of thrust to drag for the models, coupled with possible errors in the thrust determination, made it impractical to calculate power-on total drag. However, as shown in figure 10, there appears to be no large effect of the jet flow from the base on the afterbody pressures. As a result, it has been assumed that the difference between power-on and power-off drag is due to changes in base drag only.

Figures 11, 12, and 13 present the total and base drag coefficients for the three models. The "derived" power-on total drag coefficient is simply the power-off total drag coefficient plus the difference between the power-on and power-off base drag coefficients.

For model A (fig. 11) the power-on drag is an average of 12 percent greater than the power-off drag throughout the Mach number range from 0.7 to 1.0. However, since this jet-pressure ratio (approximately 0.8) is lower than that estimated for the full-scale missile in this Mach number range, this increase in drag is probably not too representative of the full-scale missile.

For model B (fig. 12) the difference between the power-on and power-off drag is small and of the order of accuracy of the data. This holds true at $M = 1.3$ where the jet-pressure ratio of the model corresponds to that of the full-scale missile.

For model C (fig. 13), the jet flow caused higher drag at Mach numbers below $M = 1.3$, and lower drags at higher Mach numbers. At $M = 1.55$, where the jet-pressure ratio of the model matches that of the full-scale missile, the results indicate a 7-percent reduction in drag. In order to make a total-drag comparison between the three models tested, it was necessary to correct the power-off total drag coefficient for the increased model fin area. This was done by the use of reference 4, and the resulting curve indicates good agreement with model B.
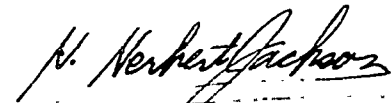
Shown in figure 14 is a comparison of the power-off base-pressure coefficient with the power-on base-pressure coefficients measured at the various p_e/p_∞ ratios tested. The power-off data are shown by an arbitrarily averaged curve. There was a maximum scatter of ± 0.004 in base-pressure coefficient over those Mach numbers (1.05 to 1.45) covered by the overlap of data from models B and C. The power-off values indicated at Mach number 1.59 are substantiated by those presented in reference 5. The data presented in reference 5, however, are for models without jet vanes and with a different A_e/A_t ratio than that obtained on test model C, so that it is impractical to make any comparison of power-on data.
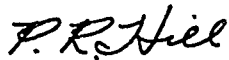
CONCLUSIONS

Three 1/5-scale models of the Hermes A-3A missile have been flown to determine the power-on drag corresponding to the missile flight altitudes and Mach numbers.

The results indicate that the power-on drag of the missile should be the same as the power-off drag at Mach number 1.3 and slightly less than the power-off drag at Mach number 1.55.

Langley Aeronautical Laboratory,
     National Advisory Committee for Aeronautics,
          Langley Field, Va., February 10, 1954.
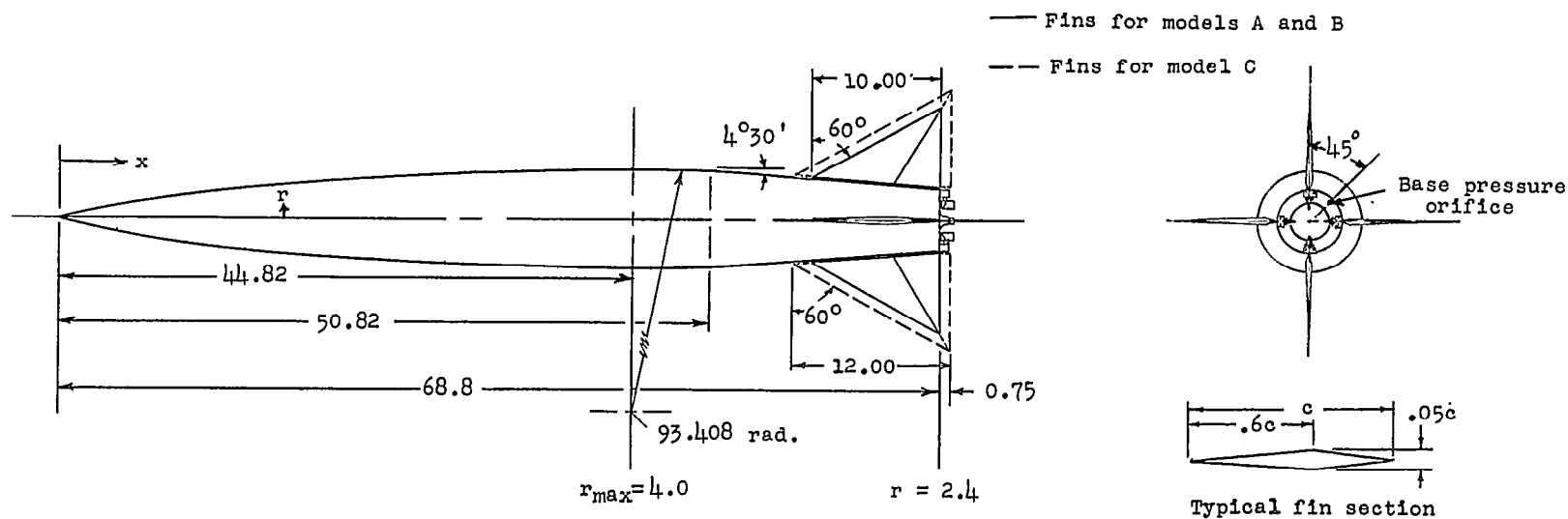
H. Herbert Jackson
Aeronautical Research Scientist

Approved: P. R. Hill

for Joseph A. Shortal
     Chief of Pilotless Aircraft Research Division

mhg

REFERENCES

1. Hayes, W. S., and McCabe, A. P.: Preliminary Aerodynamic Analysis of Nike-47 Firing Test. Rep. No. SM-13474, Douglas Aircraft Co., Inc., Feb. 1, 1949.

2. Tangren, R. F.: An Analysis of the Aerodynamic Data Obtained During the First Three CORPORAL E Firing Tests. Progress Rep. No. 4-62 (Contract No. W-04-200-ORD-455, Ord. Dept.), Jet Propulsion Lab., C.I.T., Mar. 29, 1948.

3. Wallskog, Harvey A., and Hart, Roger G.: Investigation of the Drag of Blunt-Nosed Bodies of Revolution in Free Flight at Mach Numbers From 0.6 to 2.3. NACA RM L53D14a, 1953.

4. Welsh, Clement J.: Results of Flight Tests to Determine the Zero-Lift Drag Characteristics of a 60° Delta Wing With NACA 65-006 Airfoil Section and Various Double-Wedge Sections at Mach Numbers From 0.7 to 1.6. NACA RM L50F01, 1950.

5. de Moraes, Carlos A., and Nowitzky, Albin M.: Experimental Effects of Propulsive Jets and Afterbody Configurations on the Zero-Lift Drag of Bodies of Revolution at a Mach Number of 1.59. NACA RM L54C16, 1954.

Fins for models A and B
Fins for model C

Base pressure orifice

10.00
4°30'
60°
45°
60°
12.00
0.75

44.82
50.82
68.8
93.408 rad.

$r_{max} = 4.0$ $r = 2.4$

c
.6c   .05c

Typical fin section

Nose shape equation:

$$r = \frac{d}{2}\sqrt{\frac{1}{\pi}(\phi - \frac{1}{2}\sin 2\phi + C_1 \sin^3\phi)}$$

where   d   maximum diameter

$\phi = \cos^{-1}(1 - \frac{2x}{\ell})$

ℓ total length of nose (44.82)

C_1 constant ($\frac{1}{3}$ for given volume and ℓ)

Figure 1.- External configuration of 1/5-scale Hermes A-3A free-flight
test models. Dimensions are in inches.
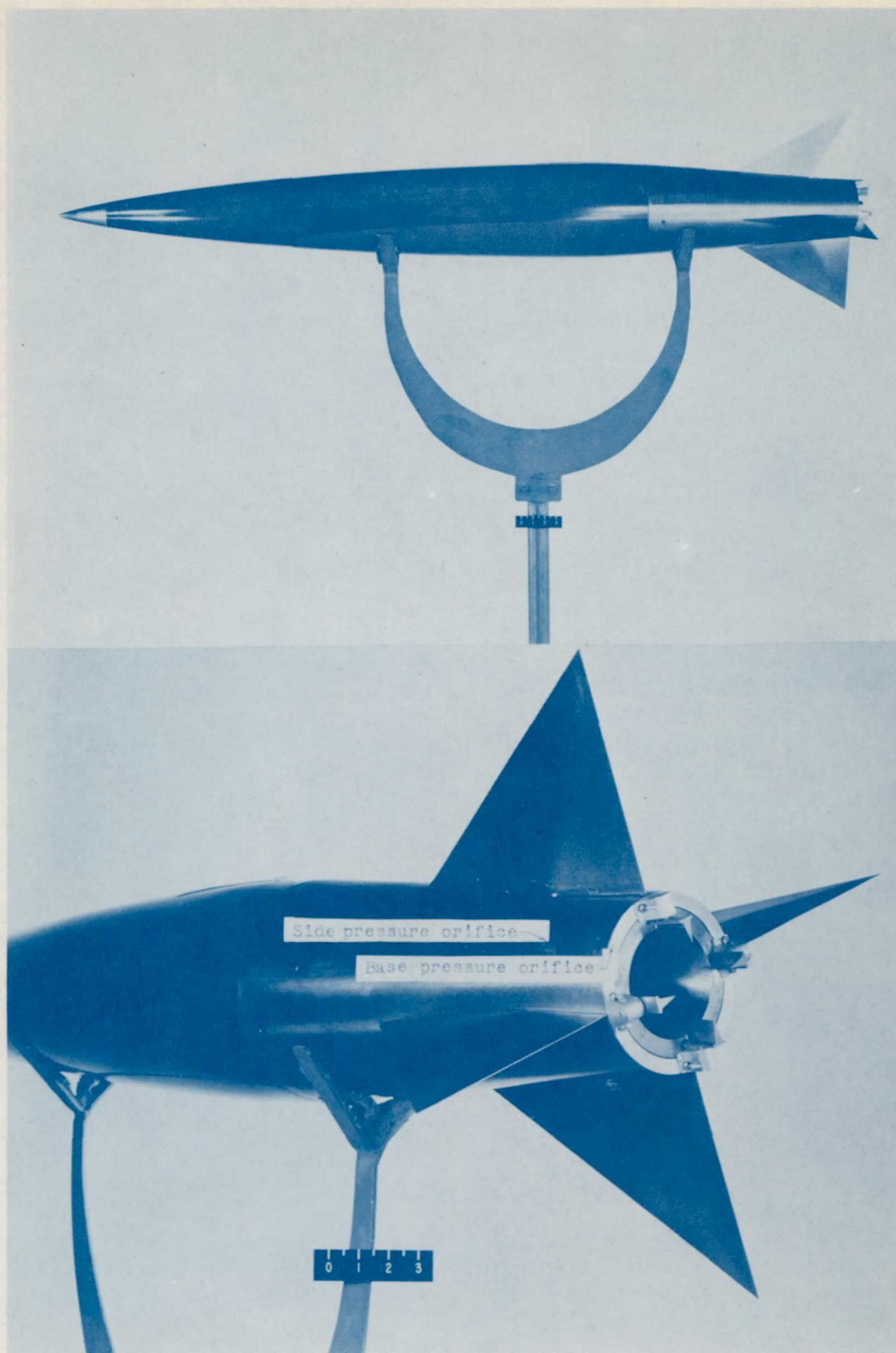
Figure 2.- General views of test model B.

L-83285
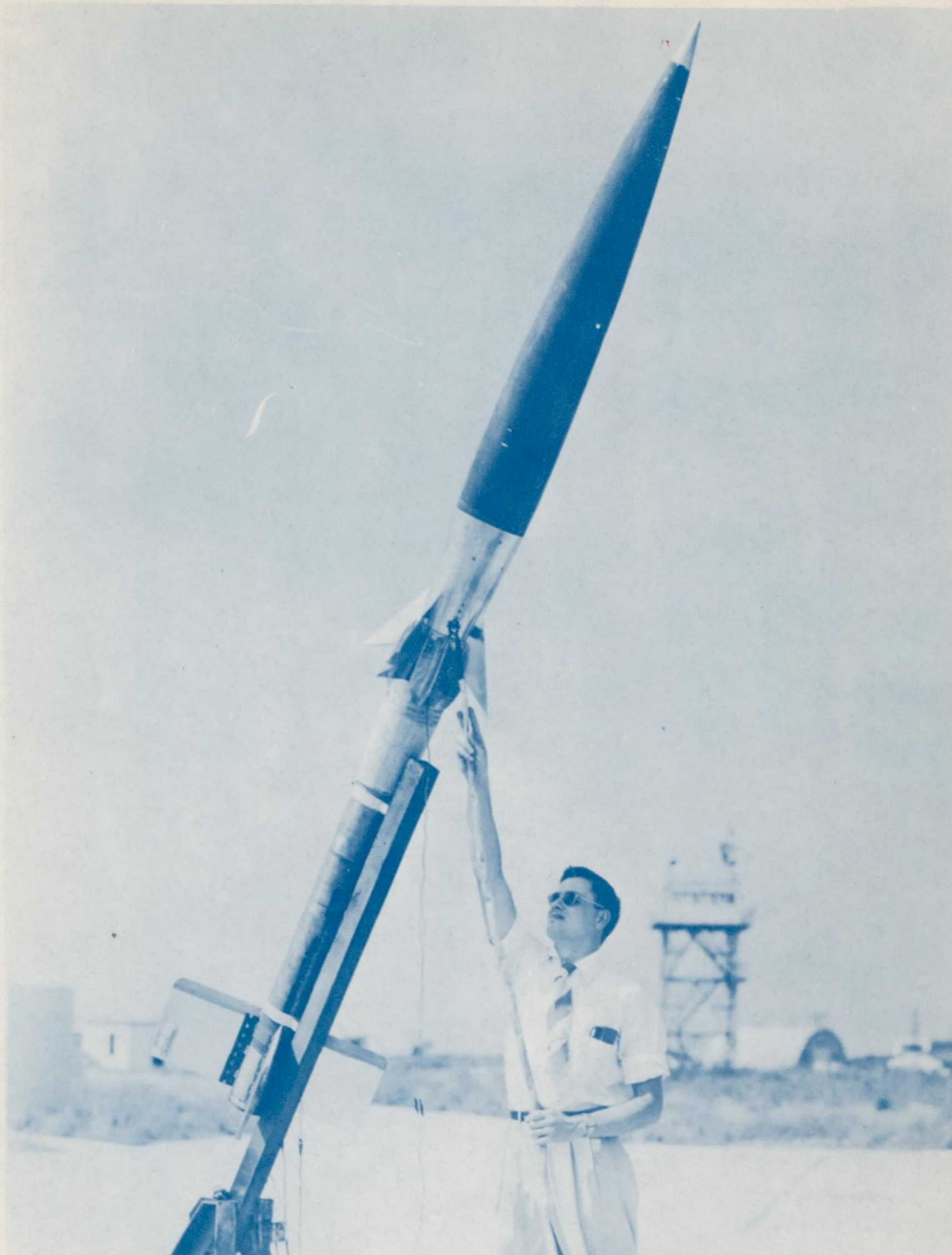
L-71819

Figure 3.- Typical model-booster arrangement on launching stand. Model B
with 5-inch HVAR lightweight booster.

After static test
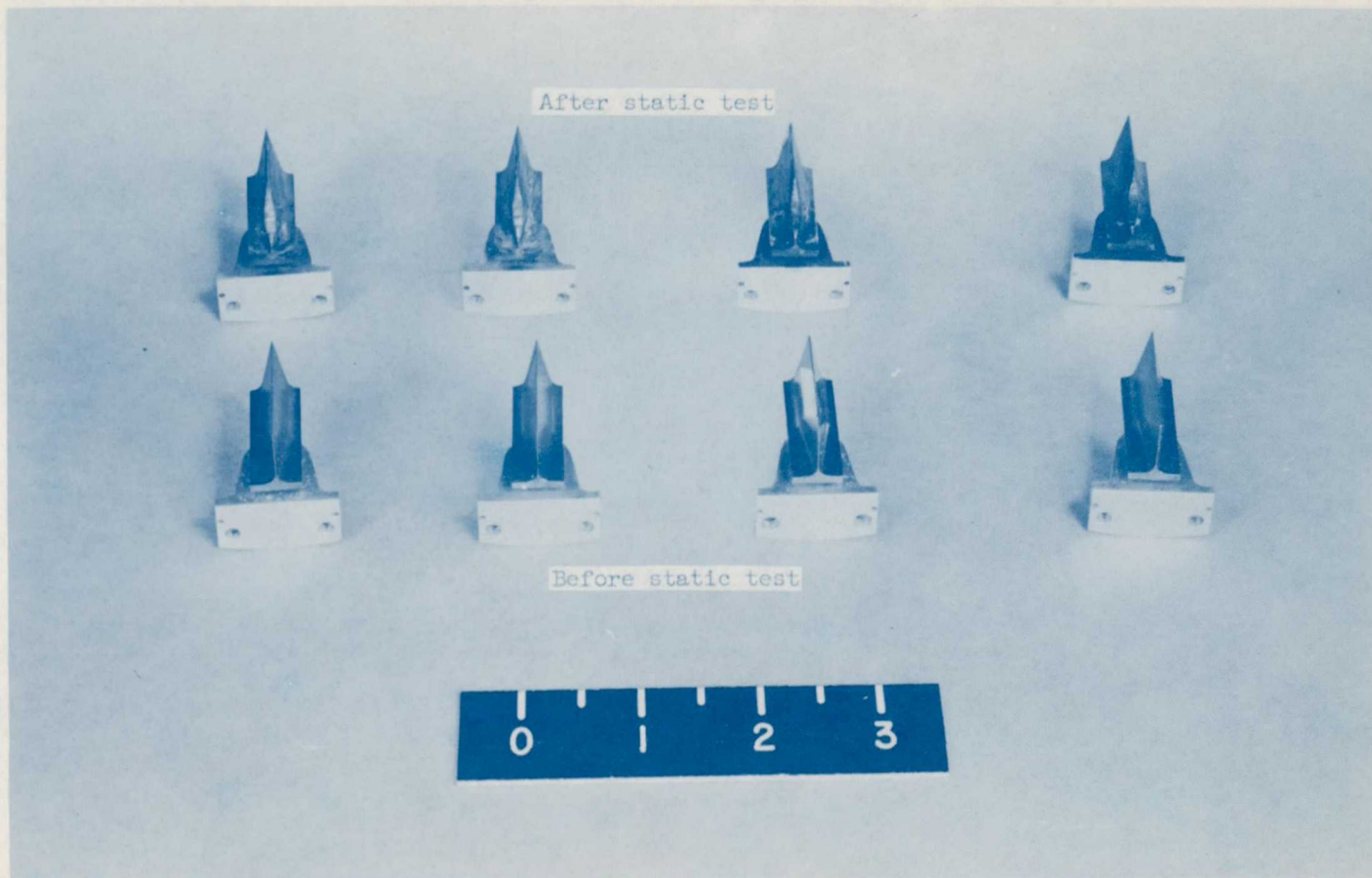
Before static test

L-71335.1

(a) Comparison of vanes before and after static test
of sustainer motor.

Figure 4.- Effect of jet on jet vanes.

Direction of jet

Area loss due to erosion and melting

Oxidation of metal

Surface blued

Slight buildup of metal
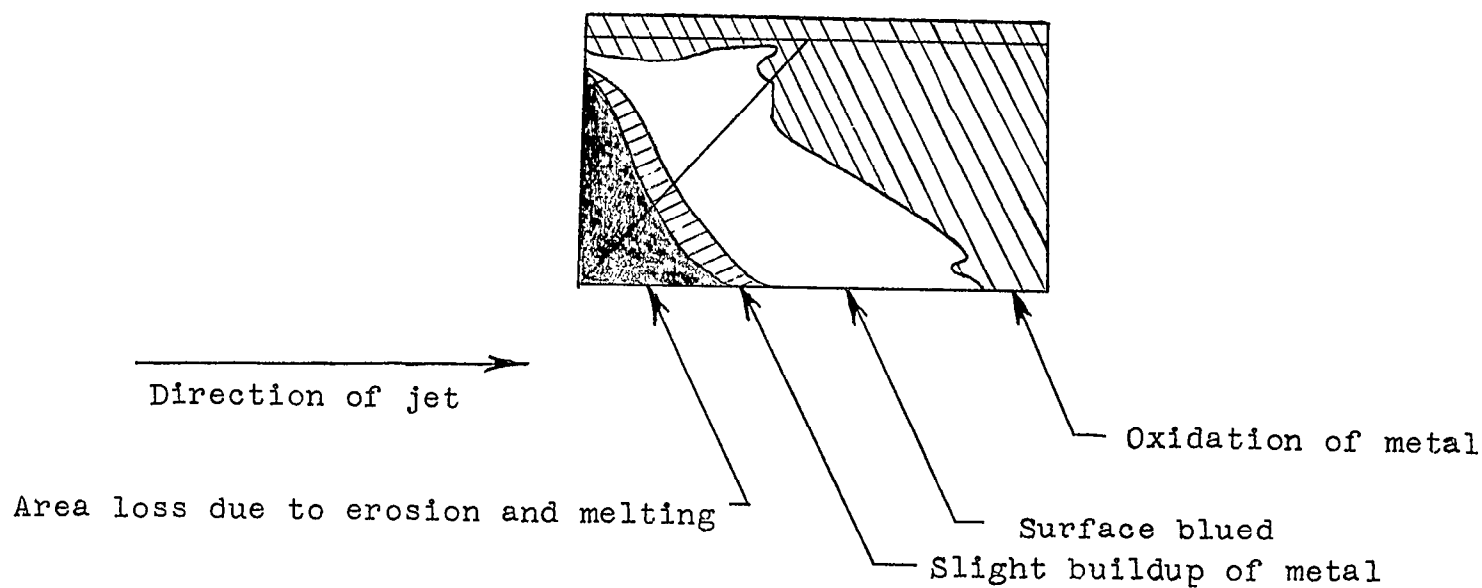
(b) Sketch of jet vane showing erosion, oxidation,
and melting caused by rocket jet.

Figure 4.- Concluded.
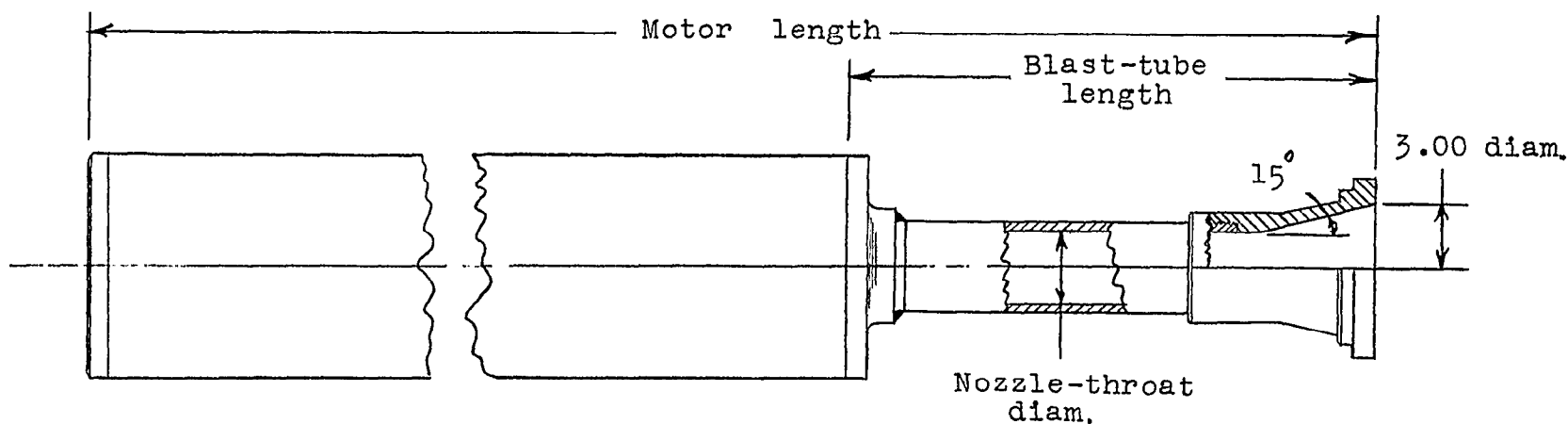
Model	Motor length	Blast-tube length	Nozzle-throat diam.	Nozzle area ratio, A_e/A_t	Burning time, sec
A	38.957	11.332	1.510	3.95	4.4
B	37.832	9.949	1.680	3.19	3.3
C	38.882	7.740	1.635	2.38	3.1

Figure 5.- Various 5-inch Cordite sustainer modifications utilized in
the test models. Dimensions are in inches.
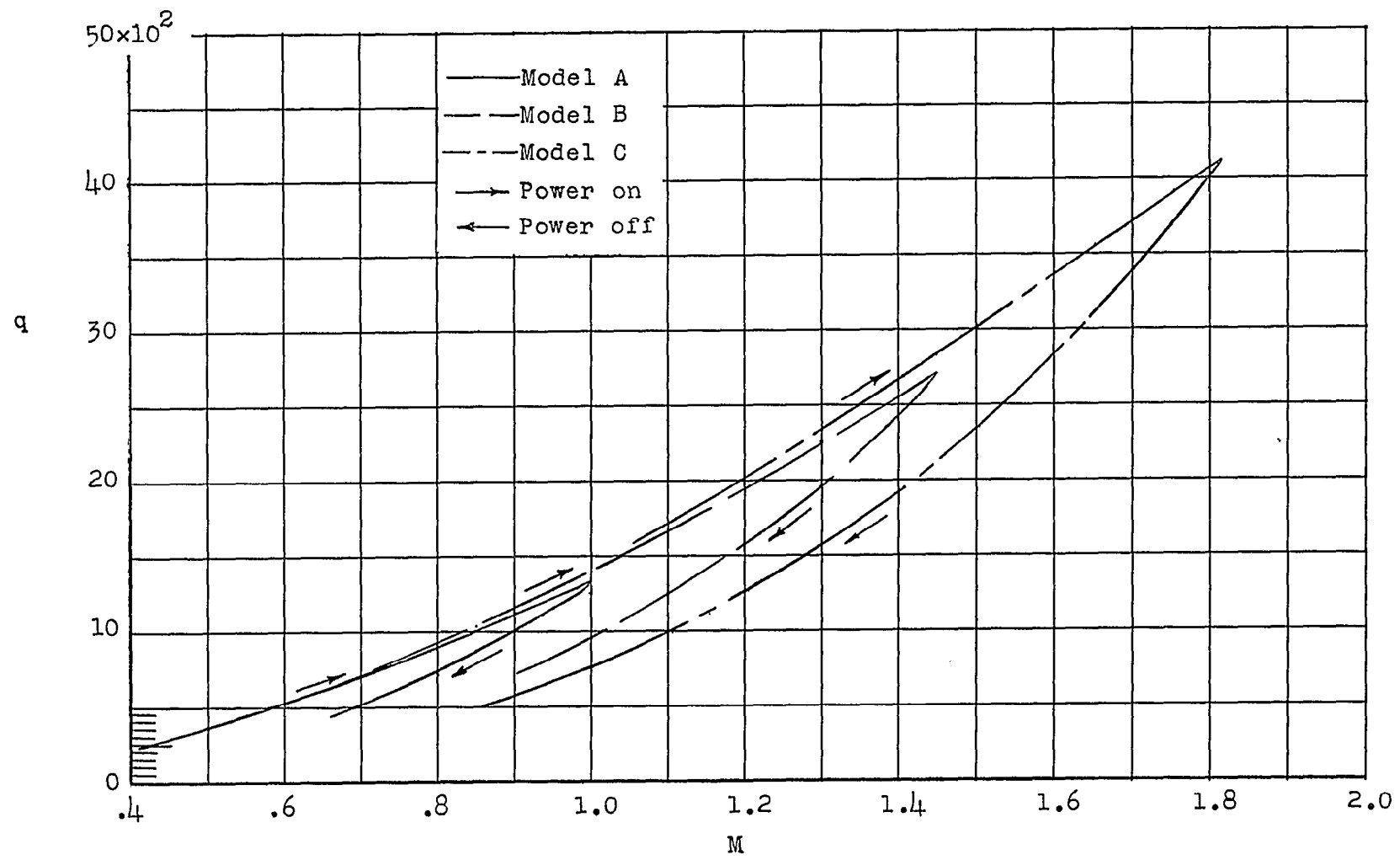
Figure 6.- Variation of dynamic pressure with Mach number for the test models.
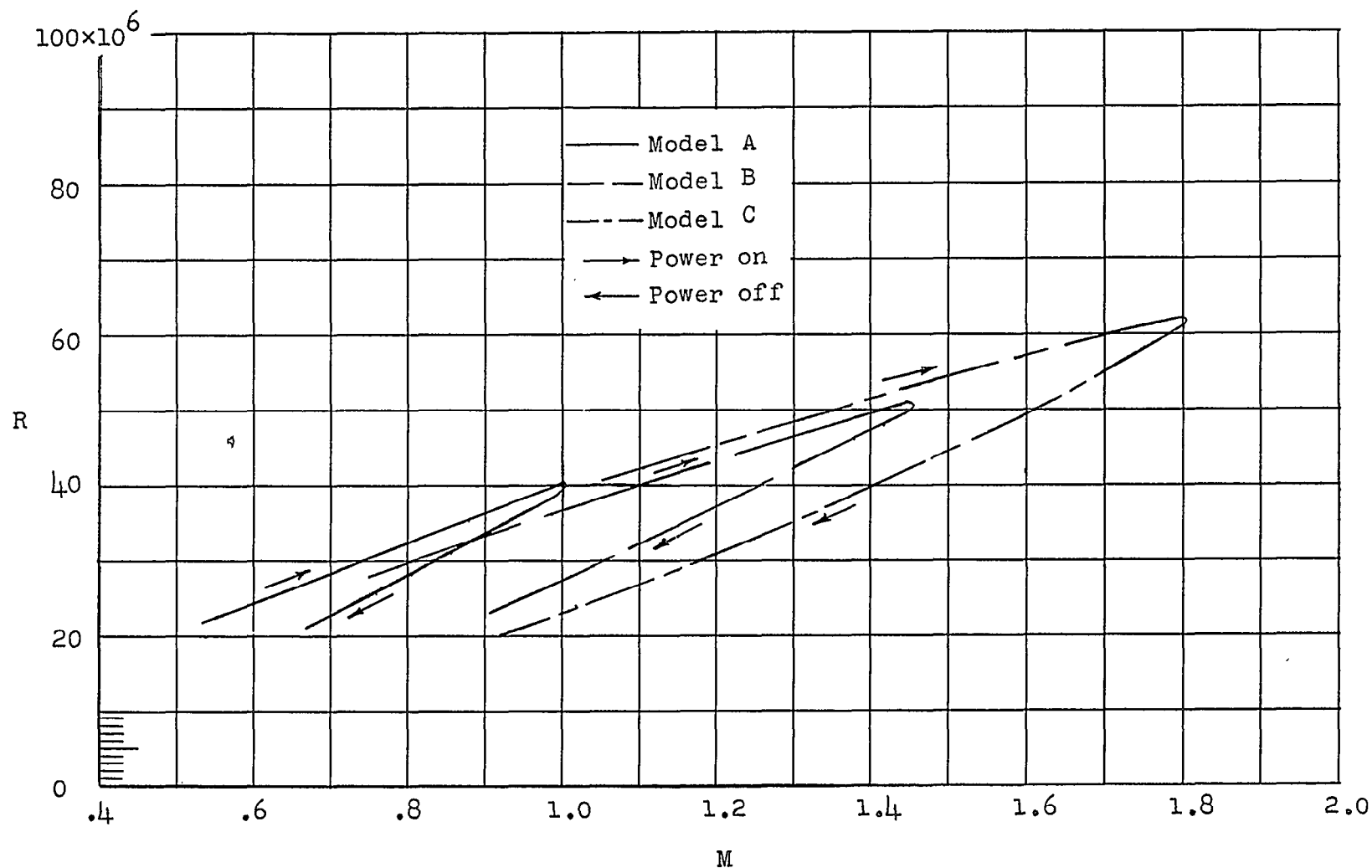
Figure 7.- Variation of Reynolds number with Mach number for the test models. Reynolds number is based on total body length.
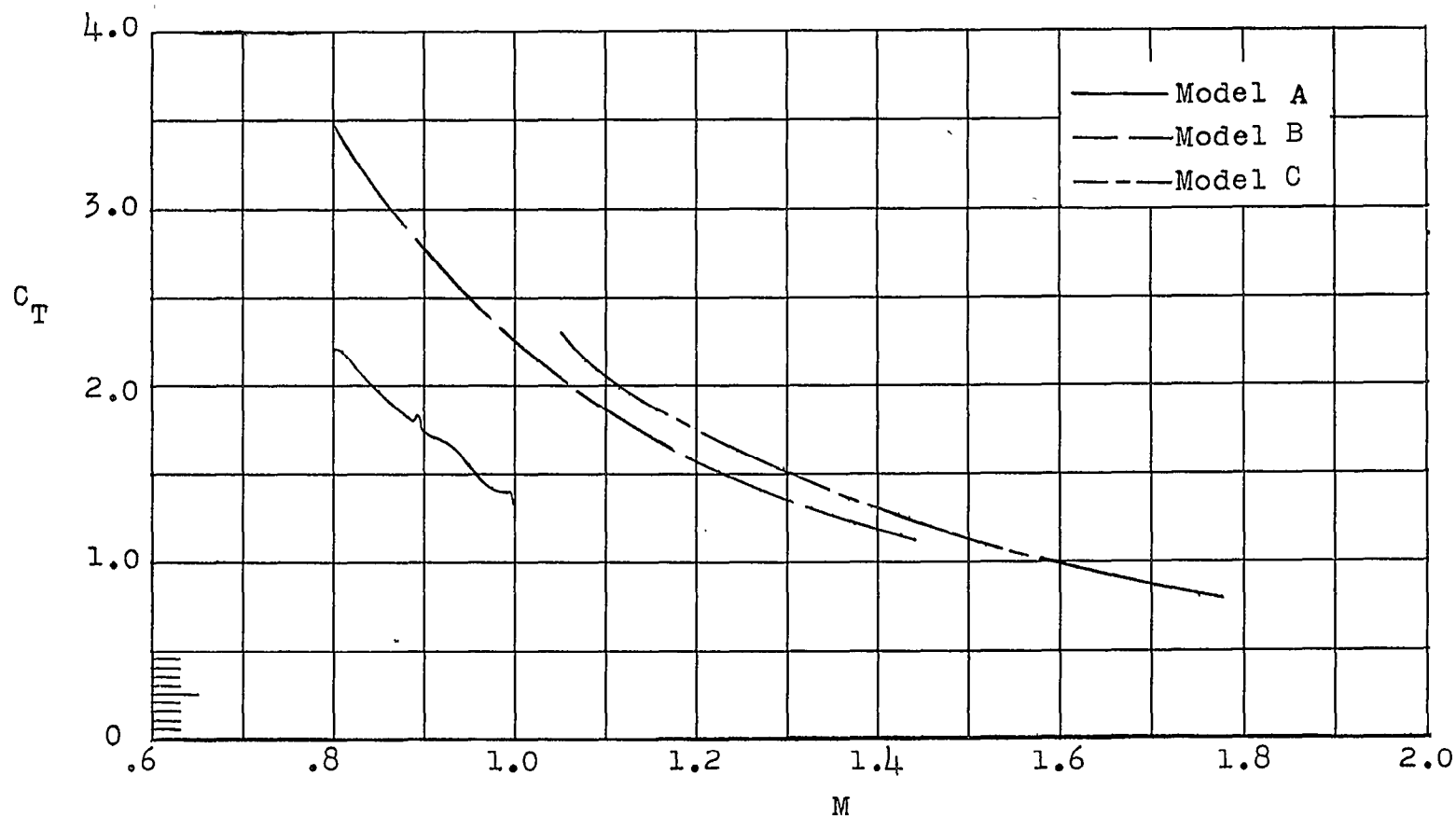
Figure 8.- Variation of thrust coefficient with Mach number for the test models. Thrust coefficient is based on body frontal area.
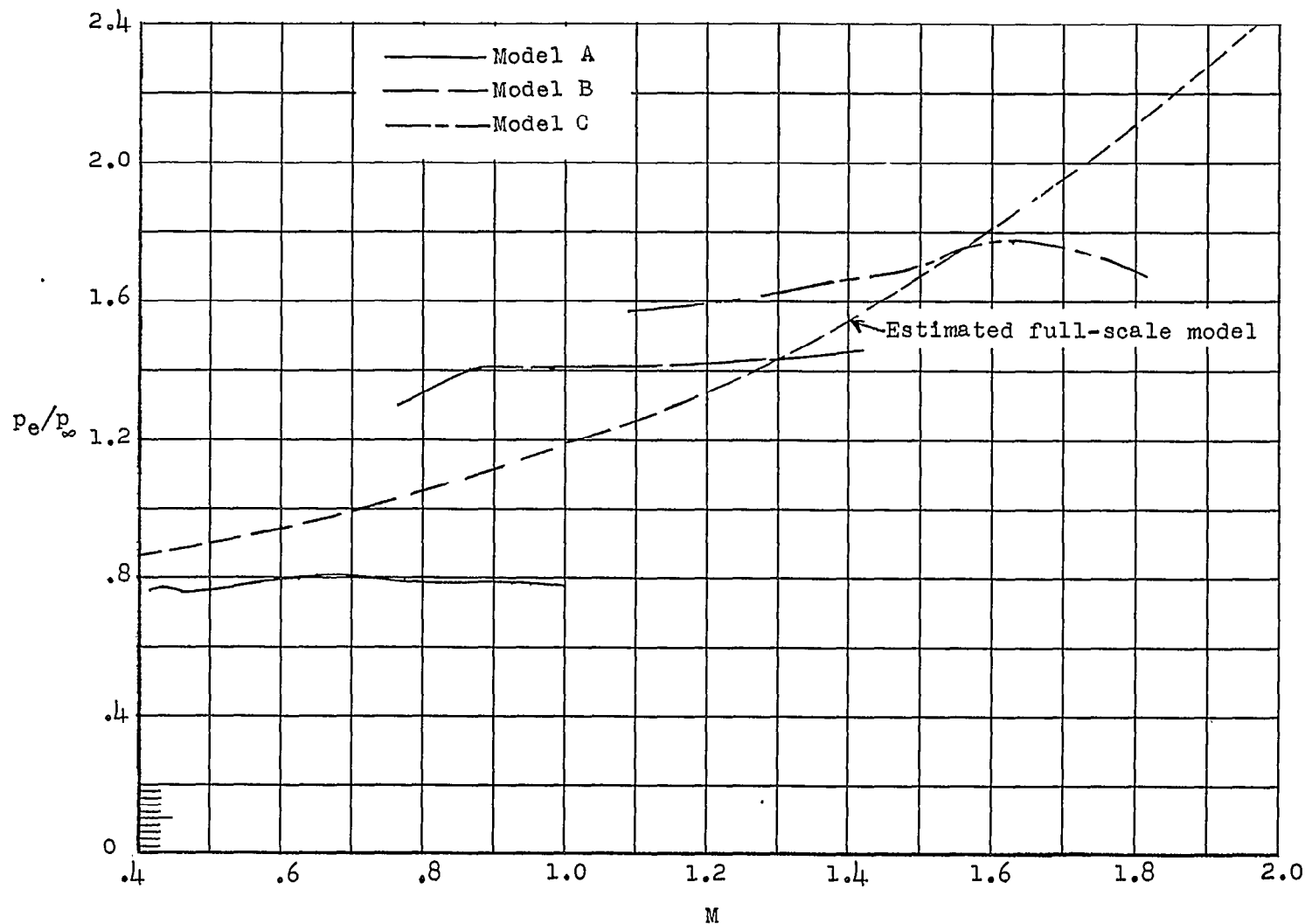
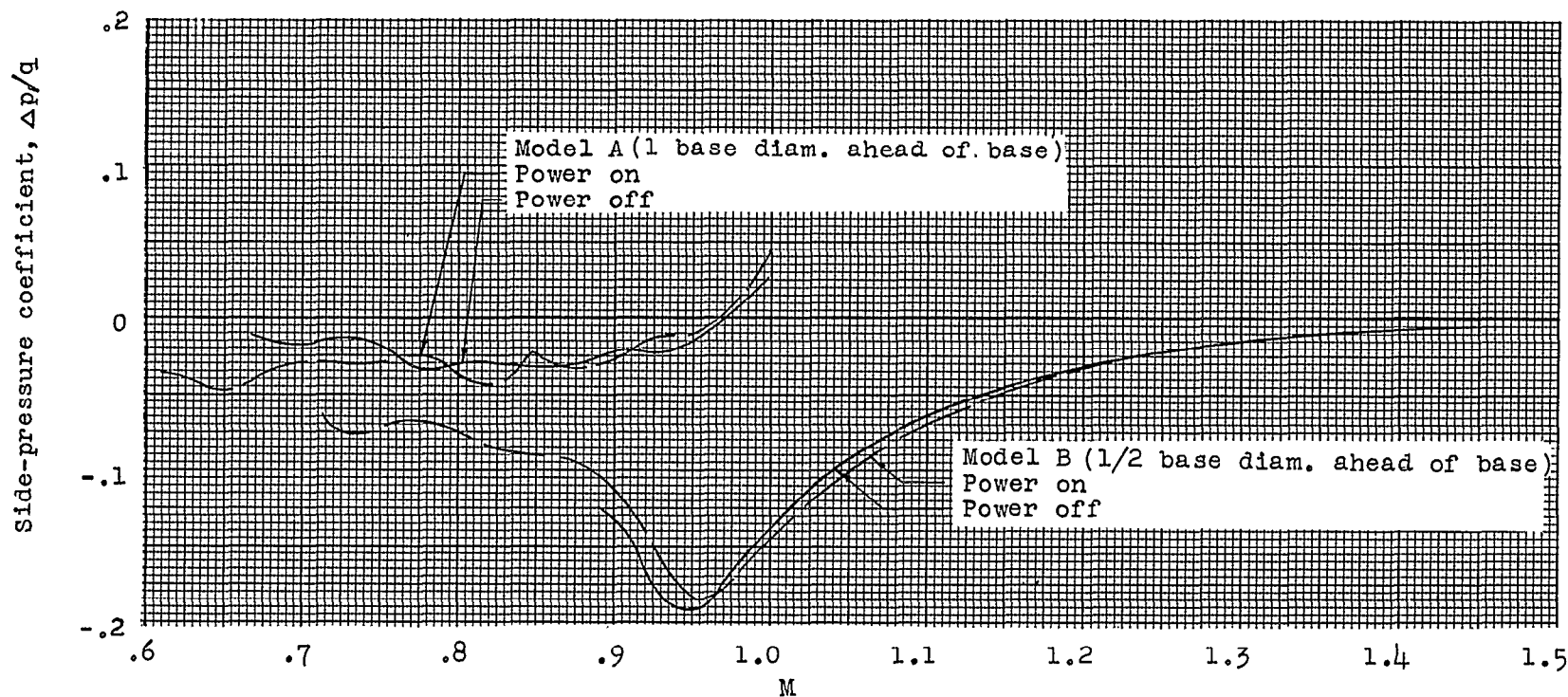Figure 9.- Variation with Mach number of the ratio of exit pressure to free-stream pressure for the test models.

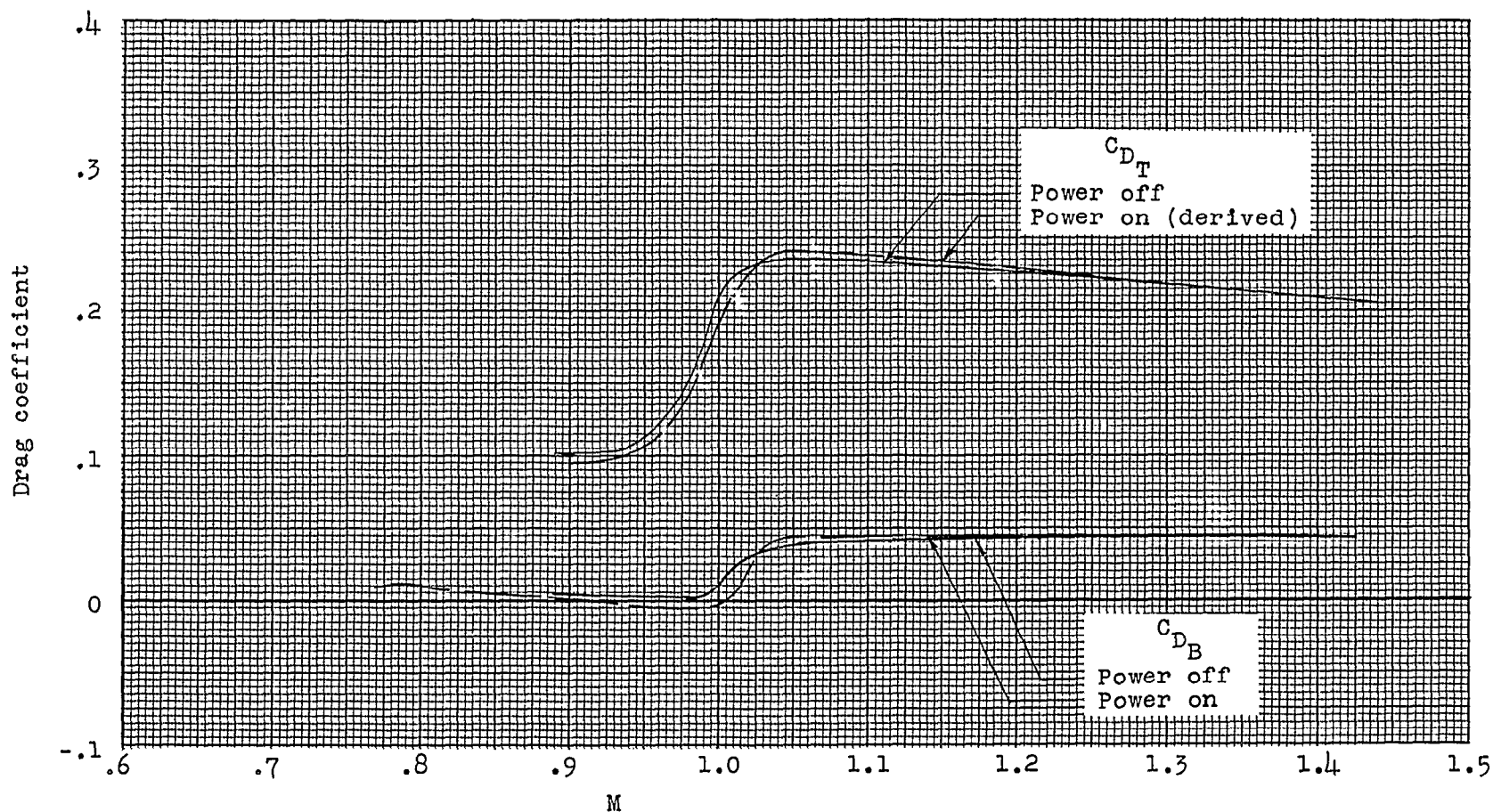Figure 10.- Variation of side-pressure coefficient with Mach number for test models A and B.
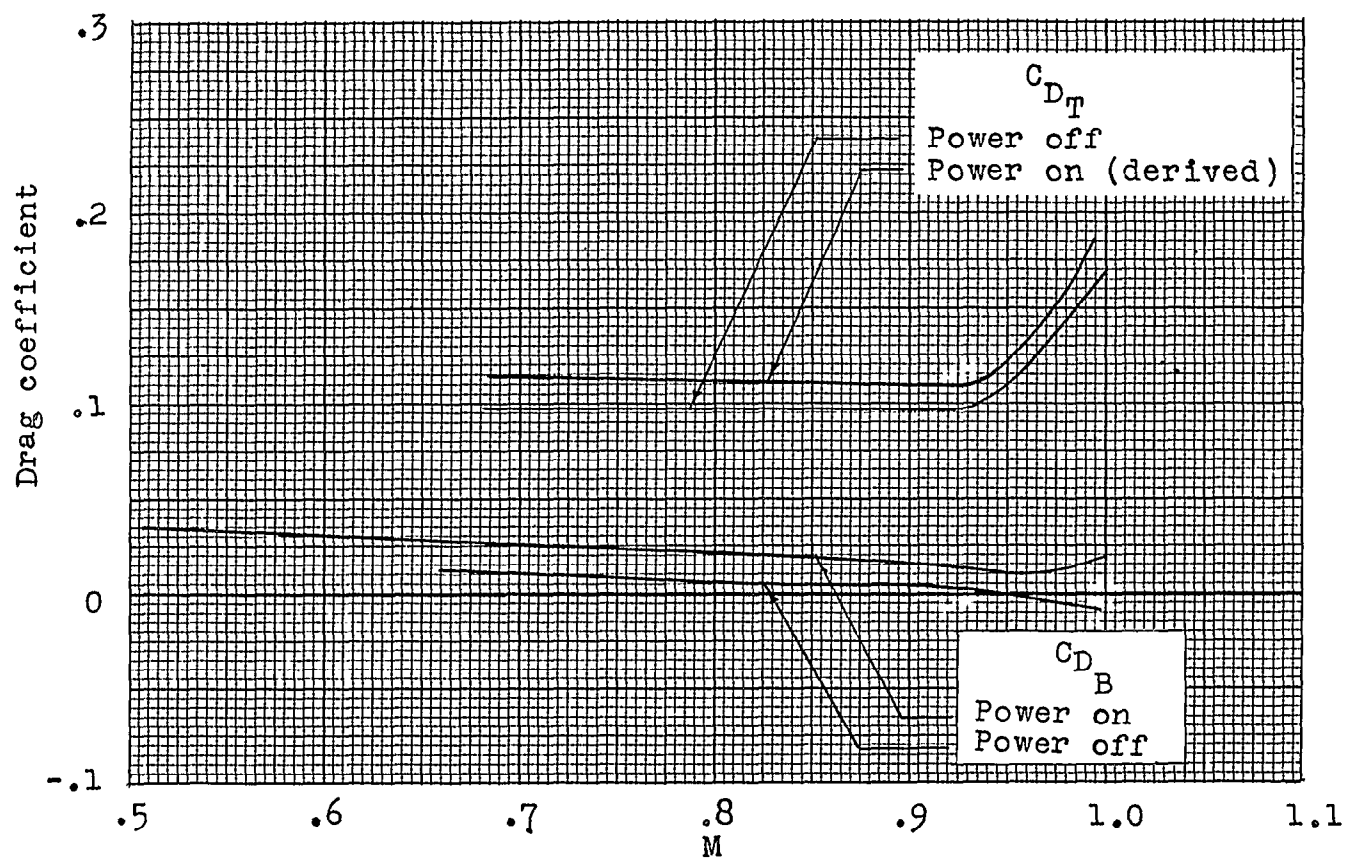
Figure 11.- Variation of total drag coefficient and base drag coefficient
(power on and power off) with Mach number for test model A. Coeffi-
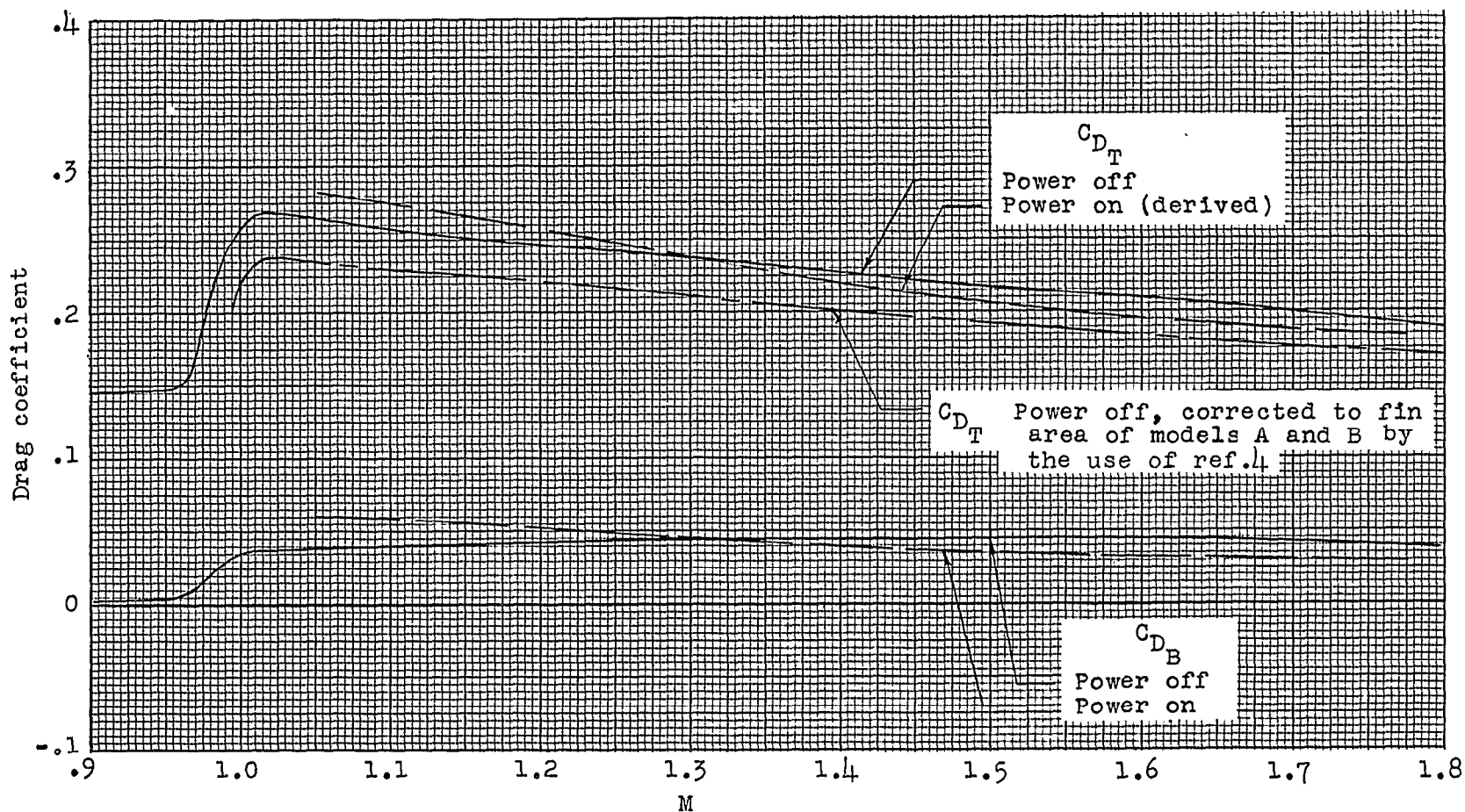cients are based on body frontal area.

Figure 12.- Variation of total drag coefficient and base drag coefficient (power on and power off) with Mach number for test model B. Coefficients are based on body frontal area.

454013

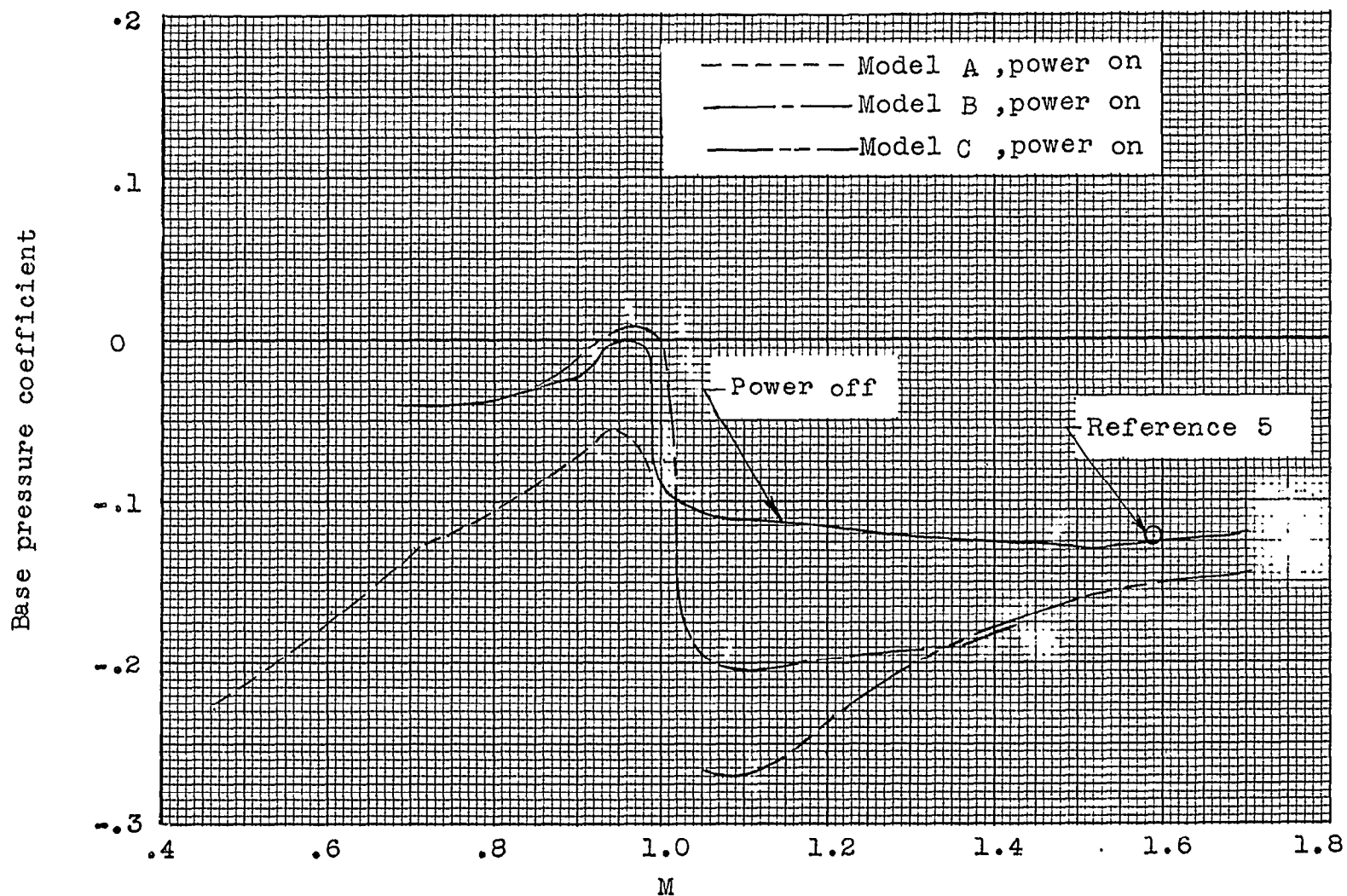Figure 13.- Variation of total drag coefficient and base drag coefficient
(power on and power off) with Mach number for test model C. Coeffi-
cients are based on body frontal area.

Figure 14.- Variation of base pressure coefficient (power on and power off) with Mach number for the test models.